

W-SHAPED SOLITONS UNDER INHOMOGENEOUS SELF- DEFOCUSING KERR NONLINEARITY

XUZHEN GAO¹, JINCHENG SHI², MILIVOJ R. BELIĆ³, JUNBO CHEN⁴, JIAWEI LI⁵,
LIANGWEI ZENG^{6,7}, AND XING ZHU⁶

¹ Department of Physics, Lyuliang University, Lishi, Shanxi 033001, China

² 54th Research Institute of CETC, Shijiazhuang 050011, China, jinchengshi1989@hotmail.com

³ Division of Arts and Sciences, Texas A&M University at Qatar, 23874 Doha, Qatar

⁴ School of Physics and Electronic Engineering, Jiaying University, Meizhou 514015, China

⁵ Key Laboratory for Physical Electronics and Devices of the Ministry of Education & Shaanxi Key
Lab of Information Photonic Technique, Xi'an Jiaotong University, Xi'an 710049, China

⁶ Department of Basic Courses, Guangzhou Maritime University, Guangzhou 510725, China

⁷ College of Physics and Optoelectronic Engineering, Shenzhen University, Shenzhen 518060, China

Received: 23.12.2023

Abstract. We demonstrate W-shaped solitons sustained under the inhomogeneous self-defocusing Kerr nonlinearity in the nonlinear Schrödinger equation. These solitons are dark or gray beams that ride on a constant background. We obtain different types of W-shaped solitons when the parameters in the equation are set suitably. All W-shaped solitons found are stable, established by the linear stability analysis, and checked by direct numerical simulation. Power defect arising in these soliton families is also investigated, and we find that the power defect change with the propagation constant is nearly linear. Besides standard perturbed propagation, we also display propagation with modulated parameters and find that the sudden variation of the appropriate parameter leads to unacceptable distortions and instability in the solution, while the gradual change of the parameter restores regular stable behavior.

Keywords: W-shaped solitons, Kerr nonlinearity, self-defocusing, Schrödinger equation

UDC: 535.32

DOI: 10.3116/16091833/Ukr.J.Phys.Opt.2024. S1075

1. Introduction

This paper is dedicated to the celebration of the 60th birthday of Prof. Anjan Biswas, an esteemed and dear collaborator in the past couple of decades. Anjan's commitment to and energy spent in the solution of various problems in nonlinear evolution partial differential equations was a source of wonder and inspiration to the vast group of his collaborators. It led to the publication of many papers in the leading journals in mathematical physics that attracted tens of thousand citations.

Solitons are formed by the balance between diffraction/dispersion and nonlinearity in many fields of nonlinear physics [1-4], both in classical (such as nonlinear optics [5-8]) and quantum mechanical (such as Bose-Einstein condensation [9-12]) fields. In passing, it should be mentioned that the critical and supercritical collapse may happen in the two-dimensional (2D) and 3D focusing/defocusing nonlinearities, respectively, where the bright solitons cannot be stabilized so easily [13, 14]. In general, it has been found that the dark solitons could be stabilized more easily than the bright ones. Methods to overcome or avoid such collapses or instabilities have attracted the attention of many researchers in the past few decades. One commonly used method is the inclusion of linear potentials, most often periodic potentials

(also called linear lattices) [15-18]. With linear potentials, many types of gap soliton families have been discovered, including multipole [19], vector [20], vortex [21], as well as surface gap solitons [22]. The harmonic potential was also used to generate stable solitons [23]. In addition, the nonlinear periodic potentials (also called the nonlinear lattices) have also been used to create various types of stabilized solitons [24-26], including fundamental [27], vector [28], dark [29], vortex [30] and multipole solitons [31], among others. It should be noted here that the inhomogeneous self-defocusing nonlinearity has been demonstrated to generate many types of solitons and has attracted lots of attention during the past decade [32-36]. Under such a nonlinearity, many solitons have been reported, including flat-top solitons [37], skyrmions [38], and soliton gyroscopes [39]. Recently, the multiple-ring solitons supported by the self-defocusing nonlinear media have been reported [40]. But generally, the stability problems of multidimensional solitons still persist.

In this paper, we will restrict our attention to the (1+1)D model with an inhomogeneous self-defocusing nonlinearity that supports a special kind of multichannel dark solitons, the *W*-solitons. These are an interesting type of solitons recently introduced, which are named for the shape of their profiles (resembling the letter *W*) [41-44]. It has been reported in many physical settings, even under fractional diffraction [45] or in the negative-indexed materials [46]. Strangely, there is no work on the *W*-shaped solitons in the simple Kerr (cubic) nonlinearity without any external potentials, although, as already mentioned, the dark beams can be more easily stabilized than the bright ones. This work focuses on generating stable *W*-shaped solitons supported by the inhomogeneous self-defocusing Kerr nonlinearity. The profiles, minimum values, power defect, and stability domains are studied in detail under different parameters. The ordinary and modulated propagation of such *W*-shaped solitons in our model is also discussed. It has been demonstrated that a sudden *z*-dependent change of nonlinearity can induce instabilities in *W*-shaped solitons while the gradual change restores stable propagation.

The rest of this paper is arranged as follows. In Section 2, the theoretical model and relevant methods of processing are introduced. In Section 3, numerical results for these *W*-shaped solitons are presented. Finally, we conclude this work in Section 4.

2. Theoretical model and method

The well-known nonlinear (1+1)D Schrödinger equation is used to describe the propagation of light beams under the inhomogeneous Kerr nonlinearity, written in the dimensionless form:

$$i \frac{\partial E}{\partial z} = -\frac{1}{2} \frac{\partial^2 E}{\partial x^2} + g(x)|E|^2 E. \quad (1)$$

Here, E denotes the slowly varying field amplitude, z is the propagation distance, and x is the transverse spatial coordinate. $g(x) > 0$ stands for the transversely-inhomogeneous self-defocusing Kerr (cubic) nonlinearity specified below. Selecting this nonlinearity in a simple localized form allows for the appearance of stabilized solitons.

We search for the stationary solutions of *W*-shaped solitons. That is, we look for the solutions of Eq. (1) in the form $E = U \exp(ibz)$, with the real propagation constant b . Upon substituting this trial solution into Eq. (1), one finds the corresponding stationary equation as:

$$-bU = -\frac{1}{2} \frac{\partial^2 U}{\partial x^2} + g(x)|U|^2 U. \quad (2)$$

Here, U denotes the stationary solution that does not depend on z – in other words, it is uniform or diffractionless along the propagation direction. The diffraction is canceled by nonlinearity.

To obtain the special W-shaped solitons in such a model, the inhomogeneous self-defocusing Kerr nonlinearity is chosen as:

$$g(x) = A_0 \left\{ \exp\left[-(x - x_0)^2 / (2W_0^2)\right] + \exp\left[-(x + x_0)^2 / (2W_0^2)\right] \right\} + C_0. \quad (3)$$

Here, A_0 , x_0 , W_0 , and C_0 are all positive constants, and x_0 determines the positions of two troughs or channels in the W-shaped solitons. The model is easily generalized to a multichannel form. For simplicity, $x_0=3$ is used throughout this work.

The stability of W-shaped solitons is an obvious concern and focus of this work. To investigate it, we employ the method of linear stability analysis – and then to check it, we utilize the direct numerical simulation. Here, the perturbed field amplitude is given by:

$$E = [U(x) + p(x)\exp(\lambda z) + q^*(x)\exp(\lambda^* z)]\exp(ibz), \quad (4)$$

where p and q are small perturbations, $*$ stands for the complex conjugate, and λ denotes the instability growth rate. By substituting Eq. (4) into Eq. (1), one obtains the eigenvalue problem for the instability growth rate as:

$$\begin{cases} i\lambda p = -\frac{1}{2} \frac{\partial^2 p}{\partial x^2} + bp + gU^2(2p + q), \\ i\lambda q = +\frac{1}{2} \frac{\partial^2 q}{\partial x^2} - bq - gU^2(2q + p). \end{cases} \quad (5)$$

According to Eqs. (5), the solutions for W-shaped solitons are stable only when all real parts of eigenvalues λ are less than zero.

In addition, for completeness, we discuss the power of W-shaped solitons. Note that the profile of W-shaped solitons is quite different from that of the bright solitons since their background intensity is not zero, while the background of the latter ones is zero. W-shaped solitons are dark or gray beams. The power of solitons is usually defined as $P = \int |U|^2 dx$; however, for the W-shaped solitons, one must discuss the power defect ΔP , just like that of other dark solitons. The power defect ΔP is defined by:

$$\Delta P = \int \left(|U_B|^2 - |U|^2 \right) dx, \quad (6)$$

where $|U_B|^2$ means the background intensity – the intensity at the boundary of U .

Below, we present numerical results for the W-shaped solitons. In this work, we use Newton's method to solve for the stationary solutions of W-shaped solitons and employ the finite-difference time-domain method to simulate their propagation.

3. Numerical results

Firstly, we display the profiles of W-shaped soliton families in Fig. 1. Figs. 1(a) and 1(b) report the typical intensity profiles of W-shaped solitons with different values of A_0 , in which one can see that the shapes of such solitons look like the letter W or like the Greek letter ω . In this work, we compare our stationary solutions with the Tomas-Fermi approximate (TFA) solution of the equation, which is obtained by neglecting the derivative term in Eq. (2). The red solid and blue dashed lines in panels (a, b) display the results for the numerical solution and the TFA, respectively. It is clearly seen that the profiles of our numerical results and TFA are similar for different values of A_0 , as shown in panels (a, b). By further checking Fig. 1(a, b), one

can also find that the minimum value of U will change with A_0 . Then, we plot the curves of U_{\min} versus A_0 for different values of W_0 in Fig. 1(c), where one can see that U_{\min} decreases with the increase of A_0 , and U_{\min} tends to be a constant when A_0 gets large enough. Finally, we discuss the power defect ΔP (defined by Eq. (6)) for such W-shaped solitons. In Fig. 1(d), we present the power defect versus A_0 for our numerical results and TFA by solid and dashed lines, respectively. The numerical results for $W_0=0.5, 0.8, 1.5$ are shown by blue, red, and pink lines, respectively. Obviously, according to Fig. 1(d), the curves of power defect versus A_0 for our numerical results are highly similar to the ones for TFA; that is, the power defect always increases with an increase of A_0 . The perturbed propagation of the W-shaped solitons labeled by S1 in panel (c) is reported in Fig. 5(a1).

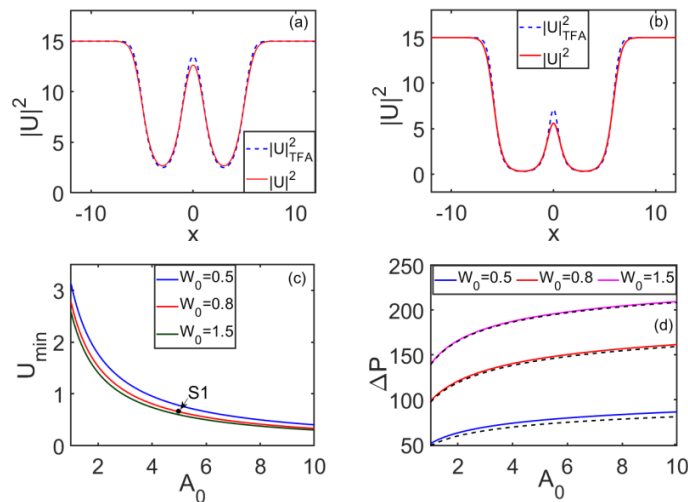


Fig. 1. Top: Intensity distributions of W-shaped dark modes, obtained by the numerical method and the TFA (red solid and blue dashed lines, respectively), supported by the potential barrier (3), for $W_0=0.8$. The other relevant parameter $A_0=1$ in (a) and $A_0=10$ in (b). Bottom: The minimum amplitude as a function of A_0 for different values of W_0 in (c). The power defect as a function of A_0 for different values of W_0 in (d). Other parameters: $C_0=0.2$ and $b=-3$ for all panels.

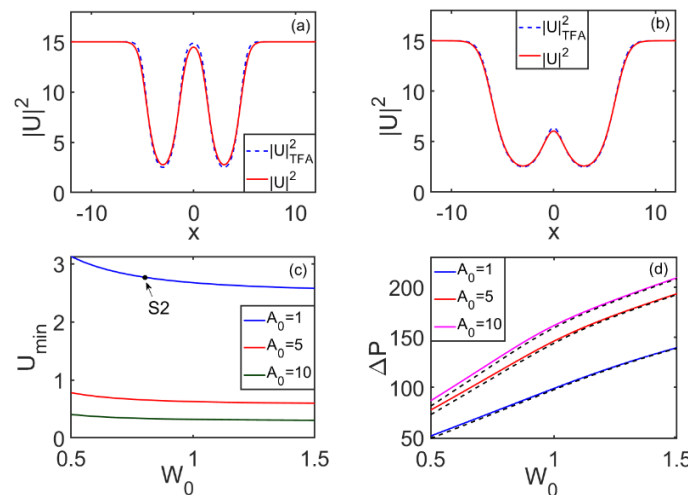


Fig. 2. Top: Same as Fig. 1, but for $A_0=1$. The other relevant parameter $W_0=0.8$ in (a) and $W_0=1.5$ in (b). Bottom: The minimum amplitude as a function of W_0 for different values of A_0 in (c). The power defect as a function of W_0 for different values of A_0 in (d). Other parameters as in Fig. 1.

Next, we discuss the profiles of W-shaped solitons for different values of W_0 . Figs. 2(a, b) display the intensity profiles of W-shaped solitons for $W_0=0.8$ and $W_0=1.5$. The red solid and blue dashed lines present the results of numerical solutions and TFA, respectively. It is obvious that the profiles of W-shaped solitons for numerical results are similar to the counterparts of TFA, as displayed in panels (a, b). Interestingly, one can also see that the width of these solitons increases with the increase of W_0 by comparing Figs. 2(a, b). Further, we present the curves of U_{\min} versus W_0 in Fig. 2(c), where the results for $A_0=1, 5$, and 10 are plotted by blue, red, and green lines, respectively. According to Fig. 2(c), U_{\min} decreases slowly with the increase of W_0 , and U_{\min} tends to be a constant when W_0 is large enough. Next, we report curves of the power defect ΔP versus W_0 for both numerical results and TFA in Fig. 2(d), where the power defect increases with the increase of W_0 for all values of A_0 . It should also be mentioned that the curves of power defect versus W_0 for numerical calculations are very close to the ones for TFA. The perturbed propagation of W-shaped solitons labeled by S2 in Fig. 2(c) is displayed in Fig. 5(a2).

Then, we analyze the profiles of W-shaped solitons for different values of C_0 . The profiles for $C_0=0.2$ and $C_0=1$ are reported in Figs. 3(a, b). In panels (a, b), the red solid and blue dashed lines display the results of numerical solutions and TFA, respectively. It is clear that the profiles for numerical calculations are similar to the ones for TFA for different values of C_0 , as shown in panels (a, b). Note also that both the maximum and minimum value of U will change with C_0 . The curves of U_{\min} versus C_0 for W-shaped solitons are presented in Fig. 3(c), in which the results for $A_0=1, 5$, and 10 are portrayed by blue, red and green lines, respectively. From Fig. 3(c) it is clear that U_{\min} decreases with the increase of C_0 , and U_{\min} tends to a constant for large values of A_0 . Finally, Fig. 3(d) displays the curves of power defect ΔP versus C_0 for both numerical results and TFA, in which the power defect decreases with the increase of C_0 for different values of A_0 . Note also that the power defect tends to a constant with the increase of C_0 when C_0 is large enough. The perturbed propagation of W-shaped solitons labeled by S3 in panel (c) is shown in Fig. 5(a3).

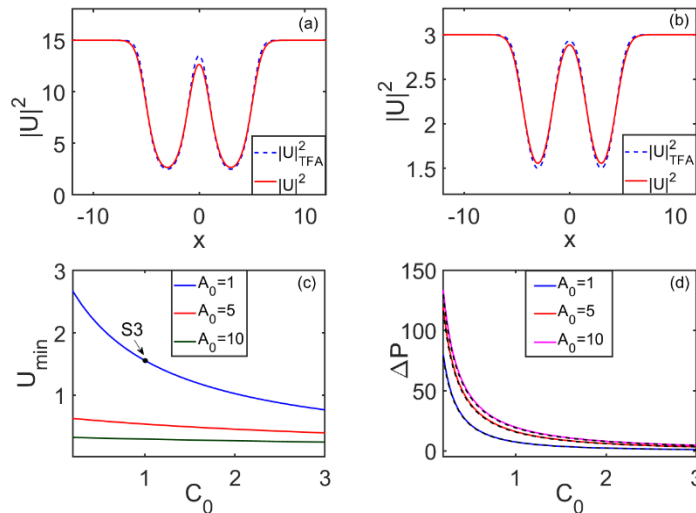


Fig. 3. Top: Same as Fig. 1, but for $A_0=1$. The other relevant parameter $C_0=0.2$ in (a) and $C_0=1$ in (b). Bottom: The minimum amplitude as a function of C_0 for different values of A_0 in (c). The power defect as a function of C_0 for different values of A_0 in (d). Other parameters: $W_0 = 0.8$ and $b=-3$ for all panels.

Now, we display the results of W-shaped solitons for different values of the propagation constant b . Figs. 4(a, b) present the profiles for $b=-3$ and $b=-8$, respectively. The red solid and blue dashed lines stand for the results of numerical solutions and TFA. Obviously, the profiles of W-shaped solitons for numerical results with different values of b are similar to their counterparts of TFA. Here, both the maximum and minimum values of U change with b , and we portray the curves of U_{\min} versus b in Fig. 4(c), where the results for $A_0=1, 5, 10$ are shown by blue, red, and green lines, respectively. According to Fig. 4(c), U_{\min} increases with the increase of b , and it increases slowly when A_0 is large enough. Finally, we display the curves of power defect ΔP versus b for both the numerical results and the TFA in Fig. 4(d), where the power defect increases linearly with the increase of $|b|$ for all values of A_0 . It should also be noted that the curves of power defect versus b for numerical calculations are consistent with their counterparts of TFA. The perturbed propagation of the W-shaped solitons labeled by S4 in Fig. 4(c) is portrayed in Fig. 5(a4).

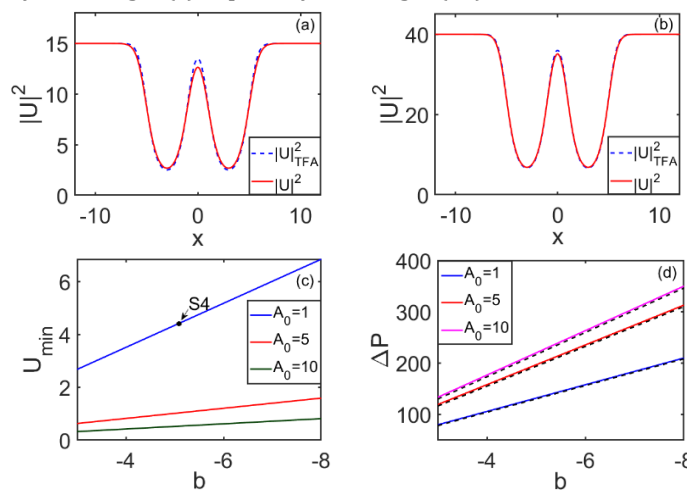


Fig. 4. Top: Same as Fig. 1, but for $A_0=1$. The other relevant parameter $b=-3$ in (a) and $b=-8$ in (b). Bottom: The minimum amplitude as a function of b for different values of A_0 in (c). The power defect as a function of b for different values of A_0 in (d). Other parameters: $W_0=0.8$, and $C_0=0.2$ for all panels.

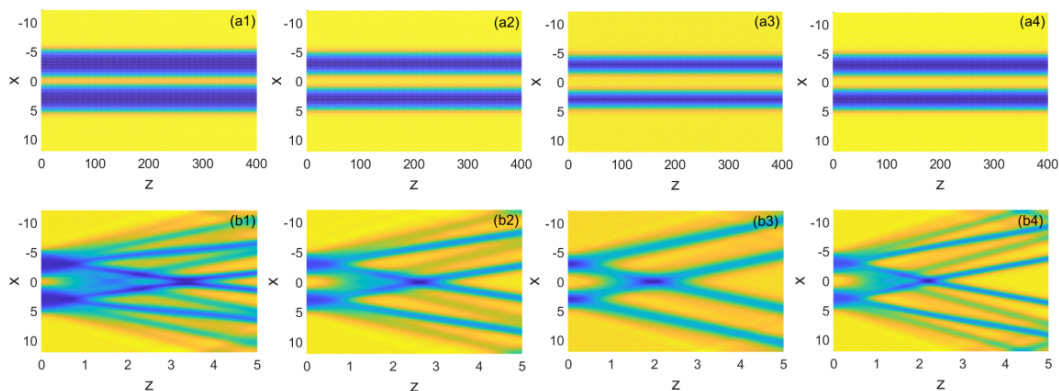


Fig. 5. The stable (top) as compared to unstable (bottom) W-shaped dark modes. $g=1$ in the bottom row so that the effect of the potential barrier to localization is diminished. Parameters of the potential barrier are $A_0=5, W_0=0.8, C_0=0.2$ and $b=-3$ in (a1) and (b1), corresponding to S1 in Fig. 1. $A_0=1, W_0=0.8, C_0=0.2$ and $b=-3$ in (a2) and (b2), corresponding to S2 in Fig. 2. $A_0=1, W_0=0.8, C_0=1$ and $b=-3$ in (a3) and (b3), corresponding to S3 in Fig. 3. $A_0=1, W_0=0.8, C_0=0.2$ and $b=-5$ in (a4) and (b4), corresponding to S4 in Fig. 4.

As already mentioned, the stability in this work is discussed by the linear stability analysis given by Eq. (5), and also checked by the direct numerical simulation of Eq. (1). We find that the W-shaped solitons obtained in our model are completely stable. We display some typical examples of such stable propagation in Fig. 5. Figs. 5(a1) – 5(a4) present four examples of stable propagation, in which all solitons keep their shapes and amplitudes during long-distance propagation. As for Figs. 5(b1) – 5(b4), their parameters are the same as in Figs. 5(a1)–5(a4), but for $g=1$, and one can easily note the distortion happening in panels (b1) –(b4). It is clear that inhomogeneous nonlinearity is a vital condition for the stable propagation of this kind of localized modes.

Finally, we discuss the results for the modulated propagation with a varying W_0 along the propagation distance. In Fig. 6(a1), we use the form of the modulated W_0 as written below:

$$W_0 = \begin{cases} 0.8 & z \leq 100, \\ 1.5 & z > 100. \end{cases} \quad (7)$$

Obviously, this form represents a sudden change in W_0 . The propagation and profiles of input and output beams based on Eq. (7) are displayed in Figs. 6(a2) – 6(a4). As seen, unacceptable distortions happen in such a propagation shown in panels (a2, a3); one can also observe that the output at the boundary is unstable and quite different from the one of the input, as displayed in panel (a4). The channels at the central position of $|U|^2$ also illustrate the same unstable behavior, as shown in panel (a5).

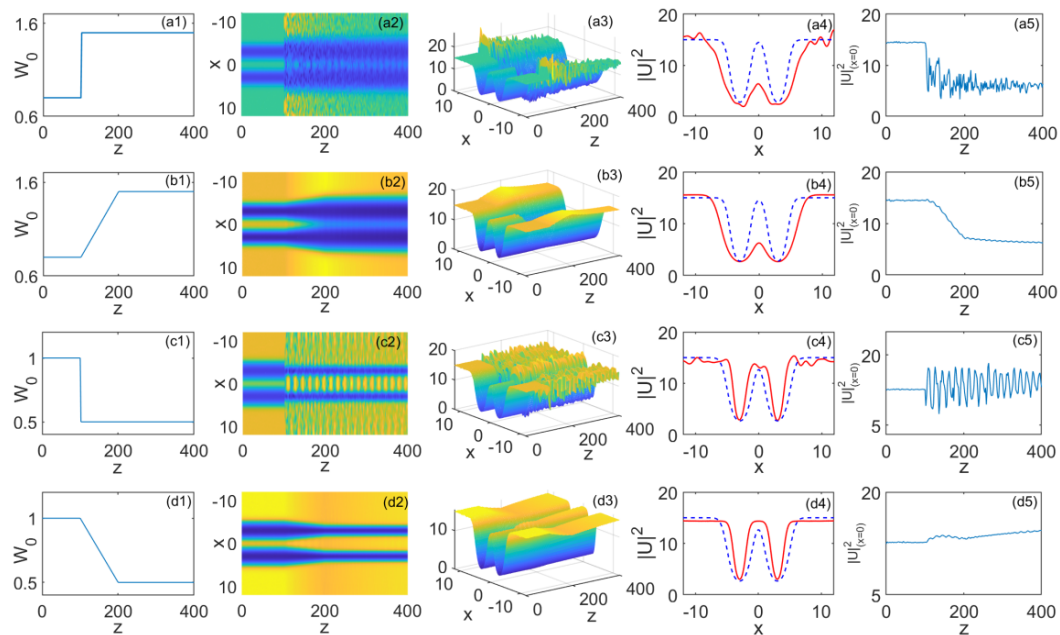


Fig. 6. (a1) Modulated W_0 along the propagation distance given by Eq. (7). Contour (a2) and the corresponding three-dimensional figure (a3) of modulated propagation based on panel (a1). (a4) Input (blue) and output (red) profiles of the propagation in (a2). Strength of $|U|^2$ at $x=0$ versus the propagation distance for propagation in (a2). (b1) – (b5) Same as panels (a1) –(a5) but for the modulated W_0 given by Eq. (8). (c1) – (c5) Same as panels (a1) – (a5) but for the modulated W_0 given by Eq. (9). (d1) – (d5) Same as panels (a1) – (a5) but for the modulated W_0 given by Eq. (10). $A_0=1$, $C_0=0.2$, and $b=-3$ for all panels.

The situation is completely different when one considers the gradual change in W_0 , as shown in Fig. 6(b1); the modulated z -dependent W_0 there is expressed by:

$$W_0 = \begin{cases} 0.8 & z \leq 100, \\ (10 + 0.7z)/100 & 100 < z \leq 200, \\ 1.5 & z > 200. \end{cases} \quad (8)$$

Under the modulation of Eq. (8), the central troughs of the soliton gradually increase with z . The corresponding propagation and profiles of input and output beams for W-shaped solitons are reported in Figs. 6(b2) – 6(b4). Different from Figs. 6(a2) – 6(a4), the propagation in Figs. 6(b2) – 6(b4) is stable, and the widths of the central parts increase gradually, following the change in the modulation, when $100 < z < 200$. The output (red line) in panel (b4) is also smooth. Such a propagation is stable, see also the value of the central portion of $|U|^2$, shown in panel (b5). Naturally, this value decreases with propagation, since the widths of two channels increase.

Now, we turn to the case when a varying W_0 decreases from 1 to 0.5. We again consider two possibilities, the sudden variation and the gradual one. In Fig. 6(c1), the form of suddenly modulated W_0 is written by:

$$W_0 = \begin{cases} 1 & z \leq 100, \\ 0.5 & z > 100. \end{cases} \quad (9)$$

The propagation and profiles of input and output based on Eq. (9) are displayed in Figs. 6(c2) – 6(c4). It is clear that such propagation suffers unacceptable distortions, as presented in panels (c2, c3). In addition, the output at the boundary is quite different from the one of the input, which can be seen in panel (c4). The irregular curve at the central position also illustrates such unstable propagation, as reported in panel (c5).

Finally, we discuss the bottom row of Fig. 6, in which the case of gradually decreasing widths of central troughs is considered. The form of W_0 in Fig. 6(d1) is expressed by:

$$W_0 = \begin{cases} 1 & z \leq 100, \\ (150 - 0.5z)/100 & 100 < z \leq 200, \\ 0.5 & z > 200. \end{cases} \quad (10)$$

Under the modulation of Eq. (10), the corresponding propagation and profiles of input and output beams for such W-shaped soliton are reported in Figs. 6(d2) – 6(d4). Similar to the results in Figs. 6(b2) – 6(b4), the propagation based on Eq. (10) is also stable, that is, the widths of the central channels decrease gradually when $100 < z < 200$. The output in panel (d4) and values of the central position of $|U|^2$ also illustrate that such propagation is stable, different from the counterparts in the top and third rows of Fig. 6. Naturally, now the widths of channels become narrower and the central intensity in panel (d5) increases during propagation. According to the results from Fig. 6, we find that the sudden variation of W_0 leads to instability and unacceptable distortions in such W-shaped solitons, and the gradual change of W_0 can lead to stable propagation.

4. Conclusion

In this work, we have demonstrated that the inhomogeneous self-defocusing Kerr nonlinearity can support a special type of dark solitons, the W-shaped solitons. The effects of different parameters on the profiles and minimum values of these solitons were studied. The

stability domains of the W-shaped solitons were also investigated, and we have found that all such solitons are completely stable, which was obtained by the linear stability analysis and also checked by the direct numerical simulation. The power defect (which is different from the power of bright solitons) was also studied in this work, and it is observed that the power defect changes with the propagation constant almost linearly. Finally, we displayed an interesting propagation with the modulated width parameter of the nonlinearity troughs and found that the sudden variation of the parameter led to unacceptable unstable distortions in W-shaped solitons, while the gradual change of the parameter led to regular stable propagation.

Funding. National Natural Science Foundation of China (62205224); Guangdong Basic and Applied Basic Research Foundation (2023A1515010865); Meizhou City Social Development Science and Technology Plan Project (2021B127); Qatar National Research Fund (NPRP 13S-0121-200126).

Disclosures. The authors declare no conflicts of interest.

Data availability. Data underlying the results presented in this paper are not publicly available at this time but may be obtained from the authors upon reasonable request.

References

1. Kartashov, Y. V., Malomed, B. A., & Torner, L. (2011). Solitons in nonlinear lattices. *Reviews of Modern Physics*, *83*(1), 247.
2. Konotop, V. V., Yang, J., & Zezyulin, D. A. (2016). Nonlinear waves in PT-symmetric systems. *Reviews of Modern Physics*, *88*(3), 035002.
3. Kartashov, Y. V., Astrakharchik, G. E., Malomed, B. A., & Torner, L. (2019). Frontiers in multidimensional self-trapping of nonlinear fields and matter. *Nature Reviews Physics*, *1*(3), 185-197.
4. Mihalache, D. (2021). Localized structures in optical and matter-wave media: a selection of recent studies. *Rom. Rep. Phys*, *73*(2), 403.
5. Zhu, X., Wang, H., Li, H., He, W., & He, Y. (2013). Two-dimensional multipeak gap solitons supported by parity-time-symmetric periodic potentials. *Optics Letters*, *38*(15), 2723-2725.
6. Yıldırım, Y., Biswas, A., Guggilla, P., Khan, S., Alshehri, H. M., & Belic, M. R. (2021). Optical solitons in fibre Bragg gratings with third-and fourth-order dispersive reflectivities. *Ukr. J. Phys. Opt.*, *22*(4), 239-254.
7. Zeng, L., Konotop, V. V., Lu, X., Cai, Y., Zhu, Q., & Li, J. (2021). Localized modes and dark solitons sustained by nonlinear defects. *Optics Letters*, *46*(9), 2216-2219.
8. Zeng, L., Belić, M. R., Mihalache, D., Li, J., Xiang, D., Zeng, X., & Zhu, X. (2023). Solitons in a coupled system of fractional nonlinear Schrödinger equations. *Physica D: Nonlinear Phenomena*, *456*, 133924.
9. Lamporesi, G., Donadello, S., Serafini, S., Dalfovo, F., & Ferrari, G. (2013). Spontaneous creation of Kibble-Zurek solitons in a Bose-Einstein condensate. *Nature Physics*, *9*(10), 656-660.
10. Henderson, G. W., Robb, G. R., Oppo, G. L., & Yao, A. M. (2022). Control of light-atom solitons and atomic transport by optical vortex beams propagating through a Bose-Einstein Condensate. *Physical Review Letters*, *129*(7), 073902.
11. Zeng, L., Zhu, Y., Malomed, B. A., Mihalache, D., Wang, Q., Long, H., Cai, X. Lu, & Li, J. (2022). Quadratic fractional solitons. *Chaos, Solitons & Fractals*, *154*, 111586.
12. Zhu, X., Xiang, D., & Zeng, L. (2023). Fundamental and multipole gap solitons in spin-orbit-coupled Bose-Einstein condensates with parity-time-symmetric Zeeman lattices. *Chaos, Solitons & Fractals*, *169*, 113317.
13. Bergé, L. (1998). Wave collapse in physics: principles and applications to light and plasma waves. *Physics Reports*, *303*(5-6), 259-370.
14. Bergé, L. (2000). Soliton stability versus collapse. *Physical Review E*, *62*(3), R3071.
15. Bartal, G., Manela, O., Cohen, O., Fleischer, J. W., & Segev, M. (2005). Observation of second-band vortex solitons in 2D photonic lattices. *Physical Review Letters*, *95*(5), 053904.
16. Desyatnikov, A. S., Ostrovskaya, E. A., Kivshar, Y. S., & Denz, C. (2003). Composite band-gap solitons in nonlinear optically induced lattices. *Physical Review Letters*, *91*(15), 153902.

17. Islam, M. J., & Atai, J. (2018). Stability of moving gap solitons in linearly coupled Bragg gratings with cubic-quintic nonlinearity. *Nonlinear Dynamics*, *91*, 2725-2733.
18. Zeng, L., Belić, M. R., Mihalache, D., Shi, J., Li, J., Li, S., Lu, X., Cai, Y. & Li, J. (2022). Families of gap solitons and their complexes in media with saturable nonlinearity and fractional diffraction. *Nonlinear Dynamics*, *108*(2), 1671-1680.
19. Zhu, X., Yang, F., Cao, S., Xie, J., & He, Y. (2020). Multipole gap solitons in fractional Schrödinger equation with parity-time-symmetric optical lattices. *Optics Express*, *28*(2), 1631-1639.
20. Kartashov, Y. V. (2013). Vector solitons in parity-time-symmetric lattices. *Optics Letters*, *38*(14), 2600-2603.
21. Lobanov, V. E., Kartashov, Y. V., & Konotop, V. V. (2014). Fundamental, multipole, and half-vortex gap solitons in spin-orbit coupled Bose-Einstein condensates. *Physical Review Letters*, *112*(18), 180403.
22. Zeng, L., Shi, J., Belić, M. R., Mihalache, D., Chen, J., Li, J., & Zhu, X. (2023). Surface gap solitons in the Schrödinger equation with quintic nonlinearity and a lattice potential. *Optics Express*, *31*(22), 35471-35483.
23. Zeng, L., Belić, M. R., Mihalache, D., Xiang, D., Wang, Q., Yang, J., & Zhu, X. (2023). Triangular bright solitons in nonlinear optics and Bose-Einstein condensates. *Optics Express*, *31*(6), 9563-9578.
24. Kartashov, Y. V., Malomed, B. A., Vysloukh, V. A., & Torner, L. (2009). Two-dimensional solitons in nonlinear lattices. *Optics Letters*, *34*(6), 770-772.
25. Abdullaev, F. K., Kartashov, Y. V., Konotop, V. V., & Zezyulin, D. A. (2011). Solitons in PT-symmetric nonlinear lattices. *Physical Review A*, *83*(4), 041805.
26. Zeng, L., & Zeng, J. (2019). One-dimensional solitons in fractional Schrödinger equation with a spatially periodical modulated nonlinearity: nonlinear lattice. *Optics Letters*, *44*(11), 2661-2664.
27. Zeng, L., Mihalache, D., Malomed, B. A., Lu, X., Cai, Y., Zhu, Q., & Li, J. (2021). Families of fundamental and multipole solitons in a cubic-quintic nonlinear lattice in fractional dimension. *Chaos, Solitons & Fractals*, *144*, 110589.
28. Kartashov, Y. V., Malomed, B. A., Vysloukh, V. A., & Torner, L. (2009). Vector solitons in nonlinear lattices. *Optics Letters*, *34*(23), 3625-3627.
29. Zeng, L., Shi, J., Li, J., Li, J., & Wang, Q. (2022). Dark soliton families in quintic nonlinear lattices. *Optics Express*, *30*(23), 42504-42511.
30. Shi, J., Zeng, L., & Chen, J. (2023). Two-dimensional localized modes in saturable quintic nonlinear lattices. *Nonlinear Dynamics*, 1-10.
31. Zeng, L., Shi, J., Belić, M. R., Mihalache, D., Chen, J., Long, H., Lu, X., Cai, Y. & Li, J. (2023). Multipole solitons in saturable nonlinear lattices. *Nonlinear Dynamics*, *111*(4), 3665-3678.
32. Borovkova, O. V., Kartashov, Y. V., Torner, L., & Malomed, B. A. (2011). Bright solitons from defocusing nonlinearities. *Physical Review E*, *84*(3), 035602.
33. Kartashov, Y. V., Lobanov, V. E., Malomed, B. A., & Torner, L. (2012). Asymmetric solitons and domain walls supported by inhomogeneous defocusing nonlinearity. *Optics Letters*, *37*(23), 5000-5002.
34. Driben, R., Kartashov, Y. V., Malomed, B. A., Meier, T., & Torner, L. (2014). Three-dimensional hybrid vortex solitons. *New Journal of Physics*, *16*(6), 063035.
35. Driben, R., Dror, N., Malomed, B. A., & Meier, T. (2015). Multipoles and vortex multiplets in multidimensional media with inhomogeneous defocusing nonlinearity. *New Journal of Physics*, *17*(8), 083043.
36. Zeng, L., Malomed, B. A., Mihalache, D., Cai, Y., Lu, X., Zhu, Q., & Li, J. (2021). Flat-floor bubbles, dark solitons, and vortices stabilized by inhomogeneous nonlinear media. *Nonlinear Dynamics*, *106*(1), 815-830.
37. Zeng, L., Zeng, J., Kartashov, Y. V., & Malomed, B. A. (2019). Purely Kerr nonlinear model admitting flat-top solitons. *Optics Letters*, *44*(5), 1206-1209.
38. Kartashov, Y. V., Malomed, B. A., Shnir, Y., & Torner, L. (2014). Twisted toroidal vortex solitons in inhomogeneous media with repulsive nonlinearity. *Physical Review Letters*, *113*(26), 264101.
39. Driben, R., Kartashov, Y. V., Malomed, B. A., Meier, T., & Torner, L. (2014). Soliton gyroscopes in media with spatially growing repulsive nonlinearity. *Physical Review Letters*, *112*(2), 020404.
40. Zeng, L., Zhu, X., Belić, M. R., Mihalache, D., Shi, J., & Chen, J. (2023). Multiple-peak and multiple-ring solitons in the nonlinear Schrödinger equation with inhomogeneous self-defocusing nonlinearity. *Nonlinear Dynamics*, *111*(6), 5671-5680.
41. Zhao, L. C., Li, S. C., & Ling, L. (2016). W-shaped solitons generated from a weak modulation in the Sasa-Satsuma equation. *Physical Review E*, *93*(3), 032215.
42. Triki, H., Porsezian, K., Choudhuri, A., & Tchofo Dinda, P. (2017). W-shaped, bright and kink solitons in the quadratic-cubic nonlinear Schrödinger equation with time and space modulated nonlinearities and potentials. *Journal of Modern Optics*, *64*(14), 1368-1376.

43. Bendahmane, I., Triki, H., Biswas, A., Alshomrani, A. S., Zhou, Q., Moshokoa, S. P., & Belic, M. (2018). Bright, dark and W-shaped solitons with extended nonlinear Schrödinger's equation for odd and even higher-order terms. *Superlattices and Microstructures*, 114, 53-61.
44. Triki, H., Zhou, Q., & Liu, W. (2019). W-shaped solitons in inhomogeneous cigar-shaped Bose-Einstein condensates with repulsive interatomic interactions. *Laser Physics*, 29(5), 055401.
45. Zeng, L., Malomed, B. A., Mihalache, D., Cai, Y., Lu, X., Zhu, Q., & Li, J. (2021). Bubbles and W-shaped solitons in Kerr media with fractional diffraction. *Nonlinear Dynamics*, 104(4), 4253-4264.
46. Triki, H., Bensalem, C., Biswas, A., Zhou, Q., Ekici, M., Moshokoa, S. P., & Belic, M. (2019). W-shaped and bright optical solitons in negative indexed materials. *Chaos, Solitons & Fractals*, 123, 101-107.

Xuzhen Gao, Jincheng Shi, Milivoj R. Belić, Junbo Chen, Jiawei Li, Liangwei Zeng, and Xing Zhu. (2024). W-Shaped Solitons Under Inhomogeneous Self-Defocusing Kerr Nonlinearity. *Ukrainian Journal of Physical Optics*, 25(5), S1075 – S1085.
doi: 10.3116/16091833/Ukr.J.Phys.Opt.2024. S1075

Анотація. Отримано розв'язки для W-подібних солітонів, які є стійкими за умови неоднорідної самодефокуруючої нелінійності Керра в нелінійному рівнянні Шредингера. Ці солітони є темними або сірими пучками, які поширюються на постійному фоні. Отримані різні типи W-подібних солітонів, при певному встановленні параметрів рівняння. Усі W-подібні солітони є стійкими, що підтверджено лінійним аналізом стійкості, а також перевірено за допомогою прямого чисельного моделювання. Досліджено також дефект потужності, що виникає у цьому сімействі солітонів, і виявлено, що зміна дефекту потужності з константою поширення є майже лінійна. Крім стандартного поширення, продемонстровано можливість поширення з модульованими параметрами і виявлено, що раптова зміна відповідного параметра призводить до неприйнятних спотворень і нестійкості у рішенні, тоді як поступова зміна цього ж параметра відновлює стійку поведінку.

Ключові слова: W-подібні солітони, керрівська нелінійність, само-дефокусування, рівняння Шредингера